J|A|C|S COMMUNICATIONS

Published on Web 05/14/2010

Synthetic Control of Structural Order in *N*-Alkylthieno[3,4-*c*]pyrrole-4,6-dione-Based Polymers for Efficient Solar Cells

Claudia Piliego,[†] Thomas W. Holcombe,[‡] Jessica D. Douglas,[‡] Claire H. Woo,[†,§] Pierre M. Beaujuge,[†,‡] and Jean M. J. Fréchet*[,†,‡,§]

Materials Sciences Division, Lawrence Berkeley National Laboratory, Berkeley, California 94720, and Departments of Chemistry and Chemical Engineering, University of California, Berkeley, California 94720-1460

Received April 19, 2010; E-mail: frechet@berkeley.edu

Intense interdisciplinary research in the field of organic photovoltaics (OPVs) has led to a significant increase in their power conversion efficiencies (PCEs) over the past decade.[1] One of the most important advances in OPVs has been the introduction of the bulk heterojunction (BHJ) architecture,[2] in which the photoactive thin film consists of an interpenetrating blend of electron donor and electron acceptor components. Extensive research efforts have focused on improving the polymeric electron donor component of the BHJ while retaining fullerene derivatives as the electron acceptor.[3] Key developments have involved narrowing the polymer bandgap, in order to better match the optical absorption with the solar spectrum, and optimizing the energy level offsets with fullerene to achieve maximum open-circuit voltage (V_{oc}).[4] For the design of new polymers, non-energetic parameters such as those that influence the physical interaction between the bulk polymer and fullerene are also important.[5] In particular, the choice of solubilizing groups is a critical factor, yet reports that directly correlate solubilizing patterns with device performance have been limited.[6] Herein, we investigate the correlation between different alkyl substituents on *N*-alkylthieno[3,4-*c*]pyrrole-4,6-dione (TPD)-based polymers and BHJ device performance, reaching PCEs over 6.5%.

During the preparation of this Communication, Leclerc et al. reported on a linear alkyl-substituted TPD-based polymer showing PCEs on the order of 5.5%.[7] We independently synthesized a series of high-molecular-weight TPD-based polymers (**P1**−**P3**, see Figure 1a and Table 1) and identified device configurations yielding PCEs between 4% and 6.8%. By preserving the π-conjugated backbone structure while modulating the size and branching of the alkyl substituent appended to TPD, we were able to maintain consistent electronic properties among the polymers. This allowed us to focus on the specific influence of solubilizing groups on OPV performance.

The thin-film optical absorption spectra of the polymers display three maxima in the 400−700 nm range (Figure 1b). By replacing the shorter but bulkier ethylhexyl chains in **P1** with the longer but less bulky octyl side chains in **P2** and **P3**, broader and red-shifted absorption spectra with more defined vibronic structure are obtained. This is indicative of a planarization of the conjugated backbone and more efficient packing of the polymer.[8] From the onset of the absorption spectra, an optical bandgap value of about 1.7 eV was estimated for all three polymers. Cyclic voltammetry (CV) was carried out to determine the electrochemical highest occupied molecular orbital levels of **P1**−**P3**. Similar values (**P1**, 5.48 eV; **P2**, 5.57 eV; and **P3**, 5.4 eV) were found for all three materials (see Supporting Information, SI).

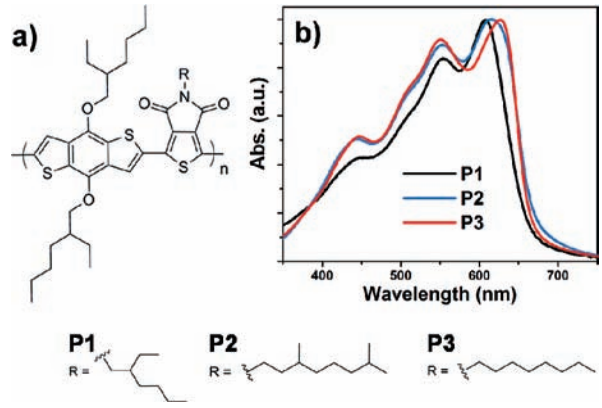

Figure 1. (a) Molecular structure of the TPD-based polymers **P1**−**P3**. (b) Normalized absorption spectra of the polymer films.

Table 1. Number-Average Molecular Weight (M_n), Polydispersity Index (PDI), and Optical Properties for **P1**−**P3**

polymer	M_n (kDa)	PDI	λ_{max} (nm)	λ_{onset} (nm)	E_g^{opt} (eV)
P1	42	2.5	608	707	1.75
P2	39	3.0	616	728	1.70
P3	35	2.7	627	716	1.73

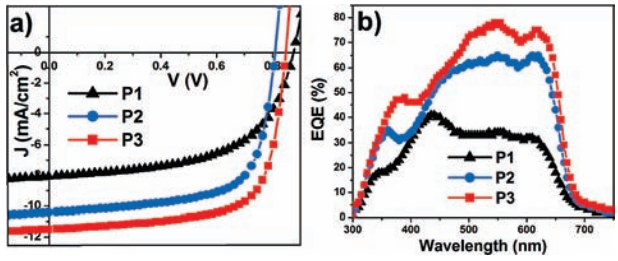

Figure 2. (a) Characteristic $J-V$ curves of bulk heterojunction solar cells fabricated from **P1**, **P2**, and **P3** under illumination of AM 1.5 G, 100 mW/cm^2. (b) External quantum efficiency spectra of **P1**-, **P2**-, and **P3**-based devices.

The photovoltaic properties of **P1**−**P3** were investigated in the device structure ITO/PEDOT:PSS/polymer:[6,6]-phenyl-C61-butyric acid methyl ester ($PC_{61}BM$)/Ca/Al. The active layers were spin-coated from chlorobenzene (CB), and in some cases a small amount of the high boiling-point additive 1,8-diiodooctane (DIO)[9] was used in order to optimize the morphology. The solubility of all three polymers in CB was high enough to allow for extensive characterization. The best $J-V$ curves are reported in Figure 2, and the average device parameters are listed in Table 2. When comparing **P1** and **P2**, it is clear that decreasing the branch length

[†] Lawrence Berkeley National Laboratory.
[‡] Department of Chemistry, University of California, Berkeley.
[§] Department of Chemical Engineering, University of California, Berkeley.

Table 2. Comparison of Photovoltaic Parameters of **P1**−**P3** in the Blend with $PC_{61}BM$

	P:$PC_{61}BM$ (wt:wt)	J_{sc} (mA/cm^2)	V_{oc} (V)	FF (%)	PCE (PCE$_{max}$) (%)
P1	1:2	−5.5	0.89	55	2.7 (2.8)
	1:2 DIO[a]	−8.1	0.87	56	3.9 (4.0)
P2	1:1.5	−7.3	0.82	62	3.7 (3.9)
	1:1.5 DIO[b]	−9.7	0.81	67	5.4 (5.7)
P3	1:1.5	−10.6	0.86	68	6.3 (6.4)
	1:1.5 DIO[b]	−11.5	0.85	68	6.6 (6.8)

[a] Devices prepared from mixed solvents chlorobenzene/1,8-diiodooctane (98/2, v/v). [b] Chlorobenzene/1,8-diiodooctane (99/1, v/v).

from two carbons to one and moving the branching point from the 2-position to the 3-position leads to an improvement in device performance. In optimized devices, the PCE increases from 3.9% for **P1**, which possesses an ethylhexyl side chain, to 5.4% for **P2**, which possesses a dimethyloctyl side chain. The elimination of branching on the TPD side chain in **P3** further enhances performance. We obtained a maximum PCE value of 6.8% in our best device with a short-circuit current $J_{sc} = 11.5$ mA/cm^2, an open-circuit voltage $V_{oc} = 0.85$ V, and a fill factor FF = 69.8% (see SI for detailed device parameters). The high FF values obtained in the best-performing devices suggest that an optimized morphology was achieved (see SI for atomic force microscopy images). The external quantum efficiency spectra of the optimized devices are shown in Figure 2b, and the maximum values are among the highest reported for solar cells based on polymer:$PC_{61}BM$ blends.

In the cases of **P1** and **P2**, the addition of DIO to the blend solution dramatically improved the performances of the devices. The use of high-boiling-point additives has been shown to promote the packing of the polymer by avoiding excessive crystallization of the fullerene.[10] We believe that this mechanism is responsible for the large enhancement in the device performances of **P1** and **P2**. In contrast, for devices realized using **P3**, the addition of DIO led to only slight improvements. These results suggest that **P3** has already reached a high level of order in the blend without DIO.

To confirm these hypotheses, we investigated the influence of the different alkyl substituents on the molecular organization in the polymer thin films using grazing incidence X-ray scattering (GIXS). Polymer blends with $PC_{61}BM$ were also examined to directly correlate microstructural order in the blends with device performance. As shown by the GIXS patterns of **P1**, **P2**, and **P3** (Figure 3a), the (010) peak corresponding to π-stacking is more prominent in the out-of-plane direction, which suggests that most of the polymer backbones are oriented parallel to the substrates (inset, Figure 3b). This face-on orientation is beneficial for charge transport in the device, and the effect is enhanced by reducing the distance d_2 (inset, Figure 3b) between the backbones. As extracted from the out-of-plane GIXS profile (Figure 3b), the value of d_2 is equal to 3.8 Å for **P1** and 3.6 Å for both **P2** and **P3**. Therefore, by replacing the ethylhexyl substituent on **P1** with the dimethyloctyl and *n*-octyl analogues on **P2** and **P3**, respectively, the π-stacking distances are reduced, which correlates well with increased device performance. The stronger intensity of the reflection coming from **P3** compared to **P2** (Figure 3a) indicates that a higher fraction of polymer backbones are oriented in the direction parallel to the substrate in the case of the **P3** film. An additional intense peak, corresponding to the reflection from the (100) crystal plane, is present in all pristine polymer films. This peak represents the distance d_1 (inset, Figure 3b), which corresponds to the lamellar

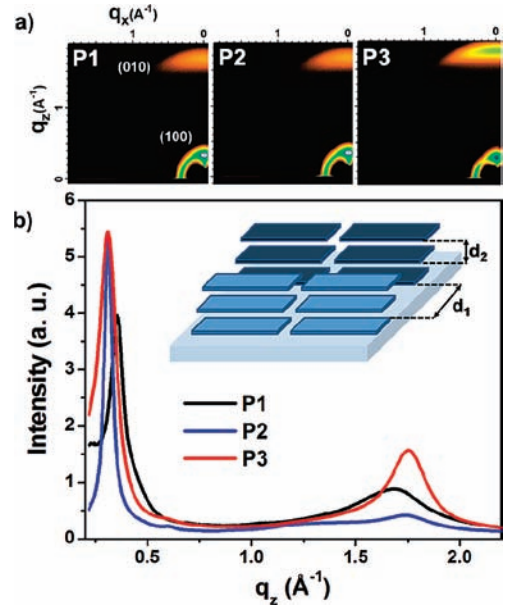

Figure 3. (a) 2D grazing incidence X-ray scattering (GIXS) patterns of films of **P1**, **P2**, and **P3**. (b) Out-of-plane linecuts of GIXS. Inset: Schematic illustration of the face-on orientation of the polymers with the backbone parallel to the substrate. The lamellar spacing and the π-stacking distance are labeled d_1 and d_2, respectively.

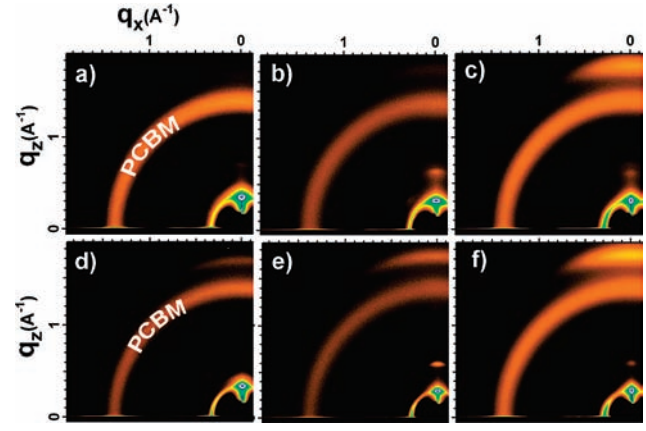

Figure 4. 2D GIXS patterns of blends of **P1** (a), **P2** (b), and **P3** (c) with $PC_{61}BM$ in the optimized condition spin-coated from chlorobenzene and **P1** (d), **P2** (e), and **P3** (f) prepared from mixed-solvent chlorobenzene/1,8-diiodooctane.

spacing in the plane. Since this distance is likely to be related to the length of the side chain, it is smaller for the hexyl derivative **P1** ($d_1 = 18.9$ Å) than for the octyl derivatives **P2** ($d_1 = 21.6$ Å) and **P3** ($d_1 = 21.2$ Å).

Interestingly, the same diffraction peaks of the pristine polymers are still visible in the 2D patterns of the blends with $PC_{61}BM$ together with the characteristic reflection of fullerene. Figure 4 shows the 2D GIXS patterns of the polymer:$PC_{61}BM$ films, obtained from the same CB and CB/DIO solutions used for device fabrication. Except for the pattern of the **P1**:$PC_{61}BM$ film without DIO (Figure 4a), the π-stacking peak is visible in all samples, indicating that the polymers are able to retain the same face-on orientation when blended with fullerene. Compared to the samples without DIO (Figure 4a−c), GIXS images of the films cast from the mixed solution CB/DIO (Figure 4d−f) show increased intensity of the π-stacking peak. This enhancement could be attributed to the

additive, which likely promotes ordering of the polymer domains. The **P3**:$PC_{61}BM$ blend from the CB/DIO solution clearly shows the highest intensity peak, indicating more extended π-stacking with respect to the other samples. The increased ordering in **P3** films is probably due to the reduction of the side-chain bulkiness, which allows the polymer to crystallize more easily, even in the presence of $PC_{61}BM$. We believe that this increased order also contributes to the higher device efficiency observed for **P3**.

By extracting the π-stacking distance from the GIXS pattern, we found that blend films containing **P2** and **P3** exhibit the same d_2 value as the pristine films (3.6 Å). From the GIXS analysis, we conclude that these TPD-based polymers are able to maintain the face-on orientation of the backbone and preserve a small π-stacking distance in the blends with fullerene.

These structures provide one of the first reports of face-on oriented polymer for solar cell applications.[11] The unique molecular packing structure is likely one of the main reasons why the TPD-based polymers are able to out-perform regioregular poly(3-hexylthiophene), which has edge-on orientation with respect to the substrate.[12] In addition to the face-on orientation of the polymer backbone, the extended microstructural order observed in the blend film of **P3** also contributes to the high performance of this polymer.

The crystallinity of the polymer affects the blend morphology, which in turn influences charge separation and charge transport in the active layer. An extensive study of these processes in TPD-based solar cells is in progress and will be the subject of a future publication. In this Communication, we focused on how the shape and size of the substituents dictate the degree and extent of the molecular packing, and we showed that these parameters have a strong influence on device performance.

In conclusion, we report the synthesis and device performance of a series of alkyl-substituted TPD-based polymers with photovoltaic responses ranging from 4.0% to 6.8%, depending on the choice of the alkyl solubilizing pattern. We demonstrate and rationalize, via GIXS analysis, how variations in the solubilizing groups impact structural order and orientation in polymer backbones, critically affecting device performance. Our results provide important insights for the design of new polymeric and molecular systems to be used in efficient solar cells.

Acknowledgment. This work was supported by the Director, Office of Science, Office of Basic Energy Sciences, Materials Sciences and Engineering Division, of the U.S. Department of Energy under Contract No. DE-AC02-05CH11231. Portions of this research were carried out at the Stanford Synchrotron Radiation Laboratory, a national user facility operated by Stanford University on behalf of the U.S. Department of Energy, Office of Basic Energy Sciences. T.W.H. and C.H.W. thank the National Science Foundation and J.D.D. thanks the Natural Sciences and Engineering Research Council of Canada for graduate research fellowships. The authors thank Dr. Jill Millstone and Dr. Justin Mynar for helpful discussions and Eric Young for the CV measurements.

Supporting Information Available: Experimental details, synthesis of the monomers and the polymers, CV of the polymers, device preparation and characterization, GIXS sample preparation and measurement procedure, and AFM images of the blend. This material is available free of charge via Internet at http://pubs.acs.org.

References

(1) (a) Thompson, B. C.; Fréchet, J. M. J. *Angew. Chem., Int. Ed.* **2008**, *47*, 58–77. (b) Kippelen, B.; Brédas, J.-L. *Energy Environ. Sci.* **2009**, *2*, 251–261. (c) Dennler, G.; Scharber, M. C.; Brabec, C. J. *Adv. Mater.* **2009**, *21*, 1323–1338. (d) Helgesen, M.; Søndergaard, R.; Krebs, F. C. *J. Mater. Chem.* **2010**, *20*, 36–60. (e) Park, S. H.; Roy, A.; Beaupré, S.; Cho, S.; Coates, N.; Moon, J. S.; Moses, D.; Leclerc, M.; Lee, K.; Heeger, A. J. *Nat. Photonics* **2009**, *3*, 297–303. (f) Liang, Y.; Xu, Z.; Xia, J.; Tsai, S.-T.; Wu, Y.; Li, G.; Ray, C.; Yu, L. *Adv. Mater.* **2010**, DOI: 10.1002/adma.200903528.

(2) (a) Yu, G.; Heeger, A. J. *J. Appl. Phys.* **1995**, *78*, 4510–4515. (b) Yu, G.; Gao, J.; Hummelen, J. C.; Wudl, F.; Heeger, A. J. *Science* **1995**, *270*, 1789–1791.

(3) (a) Blouin, N.; Michaud, A.; Leclerc, M. *Adv. Mater.* **2007**, *19*, 2295–2300. (b) Hou, J.; Chen, H.-Y.; Zhang, S.; Yang, Y. *J. Am.Chem. Soc.* **2008**, *130*, 16144–16145. (c) Huo, L.; Hou, J.; Zhang, S.; Chen, H.-Y.; Yang, Y. *Angew. Chem., Int. Ed.* **2010**, *49*, 1500–1503.

(4) (a) Scharber, M. C.; Mühlbacher, D.; Koppe, M.; Denk, P.; Waldauf, C.; Heeger, A. J.; Brabec, C. *Adv. Mater.* **2006**, *18*, 789–794. (b) Blouin, N.; Michaud, A.; Gendron, D.; Wakim, S.; Blair, E.; Neagu-Plesu, R.; Belletête, M.; Durocher, G.; Tao, Y.; Leclerc, M. *J. Am. Chem. Soc.* **2008**, *130*, 732–742. (c) Huo, L.; Hou, J.; Chen, H.-Y.; Zhang, S.; Jiang, Y.; Chen, T. L.; Yang, Y. *Macromolecules* **2009**, *42*, 6564–6571. (d) Liang, Y.; Feng, D.; Wu, Y.; Tsai, S.-T.; Rar, C.; Yu, L. *J. Am. Chem. Soc.* **2009**, *131*, 7792–7799. (e) Mondal, R.; Ko, S.; Norton, J. E.; Miyaki, N.; Becerril, H. A.; Verploegen, E.; Toney, M. F.; Brédas, J. L.; McGehee, M. D.; Bao, Z. N. *J. Mater. Chem.* **2009**, *19*, 7195–7197. (f) Zoombelt, A. P.; Fonrodona, M.; Wienk, M. M.; Sieval, B. A.; Hummelem, J. C.; Janssen, R. A. J. *Org. Lett.* **2009**, *11*, 903–906.

(5) (a) Ma, W.; Yang, C.; Gong, X.; Lee, K.; Heeger, A. J. *Adv. Funct. Mater.* **2005**, *15*, 1617–1622. (b) Mayer, A. C.; Toney, M. F.; Scully, S. R.; Rivnay, J.; Brabec, C. J.; Scharber, M.; Koppe, M.; McCulloch, I.; McGehee, M. *Adv. Funct. Mater.* **2009**, *19*, 1173–1179. (c) Cates, N. C.; Gysel, R.; Beiley, Z.; Miller, C. E.; Toney, M. F.; Heeney, M.; McCulloch, I.; McGehee, M. D. *Nano Lett.* **2009**, *9*, 4153–4157.

(6) (a) Inganäs, O.; Svensson, M.; Zhang, F.; Gadisa, A.; Persson, N. K.; Wang, X.; Andresson, M. R. *Appl. Phys. A: Mater. Sci. Process.* **2004**, *79*, 31–35. (b) Thompson, B. C.; Kim, B. J.; Kavulak, D. F.; Sivula, K.; Mauldin, C.; Fréchet, J. M. J. *Macromolecules* **2007**, *40*, 7425–7428. (c) Chen, M. H.; Hou, J.; Hong, Z.; Yang, G.; Sista, S.; Chen, L.-M.; Yang, Y. *Adv. Mater.* **2009**, *21*, 4238–4242. (d) Zoombelt, A. P.; Leene, M. A. M.; Fonrodona, M.; Nicolas, Y.; Wienk, M. M.; Janssen, R. A. J. *Polymer* **2009**, *50*, 4564–4570. (e) Wu, P.-T.; Ren, G.; Jenekhe, S. A. *Macromolecules* **2010**, *132*, 3306–3313.

(7) Zou, Y.; Najari, A.; Berrouard, P.; Beaupré, S.; Badrou, R. A.; Tao, Y.; Leclerc, M. *J. Am. Chem. Soc.* **2010**, *132*, 5330–5331.

(8) Koeckelberghs, G.; De Cremer, L.; Persoons, A.; Verbiest, T. *Macromolecules* **2007**, *40*, 4173–4181.

(9) Peet, J.; Senatore, M. L.; Heeger, A. J.; Bazan, G. C. *Adv. Mater.* **2009**, *21*, 1521–1527.

(10) Peet, J.; Cho, N. S.; Lee, S. K.; Bazan, G. C. *Macromolecules* **2008**, *41*, 8655–8659.

(11) Guo, J.; Liang, Y.; Szarko, J.; Lee, B.; Son, H. J.; Rolczynski, B. S.; Yu, L.; Chen, L. X. *J. Phys. Chem. B* **2010**, *114*, 742–748.

(12) (a) Salleo, A. *Mater. Today* **2007**, *10*, 38. (b) Woo, C. H.; Thompson, B. C.; Kim, B.; Toney, M. F.; Fréchet, J. M. J. *J. Am. Chem. Soc.* **2008**, *130*, 16324–16329.

JA103275U